Experimental Test-Bed for Multi-Vehicle Control, Navigation and Communication

Ralf Bachmayer, Naomi Ehrich Leonard*
e-mail:{ralf, naomi}@princeton.edu

12th International Symposium on Unmanned Untethered Submersible Technology, 2001

Abstract

In this paper we describe the design and evaluation of the prototype vehicle for a new test-bed developed for multi-vehicle control, navigation and communication. The vehicle is designed for high reliability and easy reconfiguration using smart sensor and actuator interfaces. It is passively stable in pitch and roll and is actuated by five thrusters. The actuators allow for full control of the remaining four degrees of freedom. We are developing the multi-vehicle test-bed to test control algorithms that demonstrate coordinated and cooperative behavior of a network of vehicles for adaptive ocean sampling and other applications. In our design of coordinating control laws, we are inspired by the remarkable capabilities of schooling fish. To illustrate, we describe a multi-vehicle approach to gradient climbing. The simple control algorithm that we present allows two vehicles that observe one another to climb a gradient under the constraint that each vehicle can only take single point measurements.

1 Introduction

During the last five years autonomous underwater vehicles (AUVs) have impressively demonstrated their usefulness to the oceanographic community [14, 15] and are increasingly used for commercial applications [9, 10]. Important successes of AUVs include bathymetric mapping and seafloor imaging. These missions are mostly preprogrammed and require only a limited amount of onboard decision making and data processing, but they translate into considerable savings in terms of man-power and ship time. With commercialization and an eventual drop in overall system costs, it is foreseeable that multiple vehicles will be deployed simultaneously to increase the sensor coverage, to shorten the survey time and for other advantages associated with economy of scale. However, there is the potential that multi-vehicle configurations can provide an even more significant contribution. With effective control design it is possible that networks of vehicles can achieve highly efficient and adaptive group capabilities from simple rules at the individual vehicle level, much like emergent intelligence in schools of fish. This could lead to improved data-processing and decision-making capabilities which could have a major impact on missions such as adaptive ocean sampling.

Biologists have studied the behavior of animal aggregations such as schools of fish and flocks of birds. They have observed complex behaviors on the group level emerging from simple rules apparent on the individual level [11, 12]. The observed behaviors allow, for example, for more efficient foraging, effective protection against predators and in some cases higher energy efficiency when flying in formation. With the observations as well as the models put forth by the biologists as motivation, we are developing decentralized control algorithms that are relatively simple on the individual vehicle level but can perform challenging tasks at the group level [7, 13]. Here we describe a multi-vehicle approach to gradient climbing and illustrate how the knowledge of near neighbor behavior can play a fundamental role.

In order to test and demonstrate coordinating control algorithms on real vehicles we are developing a multi-vehicle test-bed. Our goal is to provide the means for easily accessible experimentation; according, our test-bed will initially be operated in a freshwater tank in an indoor laboratory. This we see as an important step towards full-scale implementation of coordinating control algorithms at sea. There are a number of new and exciting challenges associated with our multi-vehicle test-bed objectives. Here, we

*The authors are with the Department of Mechanical & Aerospace Engineering, Princeton University, Princeton, NJ 08544. Research partially supported by the National Science Foundation under grant CCR-9980058 and by the Office of Naval Research under grants N00014-98-1-0649 and N00014-01-1-0526.

describe our approach to some of these and present some details on the design of our prototype "grouper" vehicle.

In Section 2 we describe our multi-vehicle approach to gradient climbing. A simple gradient climbing control law is defined where it is assumed that each vehicle can only take a single measurement at a time. We show that this control law does not in general enable a single vehicle working along to find the "source" of the gradient. However, in the two-vehicle case, we show that the vehicles are able to climb the gradient and find a source. The results are based on certain assumptions about the local interaction of the two vehicles that allow us to model the group as a connected system of two point masses. We present simulation results for the one and two-vehicle case.

In Section 3 we describe the development of the experimental test-bed. The requirements for the experimental setup are described in Section 3.1. In Section 3.2 we briefly describe the mechanical layout of the prototype vehicle. The system architecture with the outline of the vehicle's internal communication as well as the inter-vehicle and vehicle-surface communication are described in Section 3.3. We include a brief discussion of possible means of implementing decentralized and centralized control concepts. In Section 3.4 we list the basic sensor suite for the vehicles and briefly describe an optical sensor that is currently under development. Preliminary experimental results with closed-loop depth and heading control are discussed in Section 3.5.

2 Gradient following

In this section we give an example that illustrates the potential benefit of a multi-vehicle configuration over a single vehicle. We first describe a biological example that has motivated some solutions to the gradient climbing problem [4, 5]. Next we introduce the assumptions and constraints we impose on the system. Given these constraints we develop a simple control algorithm for gradient climbing. We show that if this algorithm is applied to a single vehicle, the vehicle does not in general converge on the source. In a next step we apply the same algorithm to two interacting vehicles modelled by two connected masses. Due do to the interaction between the vehicles, the vehicles are expected to find the source. We present simulations that support this claim.

2.1 Previous work on gradient following using *E. coli* model

One way to address the gradient following problem with a single vehicle was demonstrated using the Autonomous Benthic Explorer (ABE) to find the deepest spot in a lake [4]. This approach can be derived from the behavior models of flagellated bacteria like the *Escherichia coli* [1, 2]. The *E. coli* bacteria moves towards or away from certain chemicals; this behavior is referred to as chemotaxis. The mechanism used to achieve chemotaxis is *run and tumble*. This means that while the gradient is rich enough the bacteria continues for longer stretches in a forward motion before it tumbles and takes off again in a random direction. If the gradient becomes weaker the bacteria decreases the distance between the direction changes. As a net effect of this strategy the bacteria accumulates in areas of richer gradients.

2.2 Assumptions and constraints

For the remainder of this paper we consider only planar motions of the vehicle(s). A surrounding environmental quantity is represented by a time-invariant scalar field $T(\underline{x}) \in \mathbf{R}$ (e.g., bathymetry). We constrain the system to a single sensor per vehicle, such that we record $T(\underline{x})|_{\underline{x}=\underline{x}_i}$, where $\underline{x}_i$ represents the position of the vehicle at time $t = t_i$. The single point sensor measurements do not allow for a full 2D gradient measurement for a given vehicle, but the measurements provide information about the gradient along the vehicle's path. We can, therefore, approximate the successive measurements performed along a vehicle's path by projecting the spatial gradient of the scalar field onto the normalized vehicle velocity vector $\dot{\underline{x}}$. Thus, we assume

$$\nabla T_{\dot{\underline{x}}} = \nabla T \cdot \frac{\dot{\underline{x}}}{\|\dot{\underline{x}}\|} \tag{1}$$

is measured. Note that $\nabla T_{\dot{\underline{x}}} \in \mathbf{R}$. We do not allow for any direct communication between the vehicles; however, we assume that each vehicle can observe the other's position.

2.3 Single-vehicle configuration

Consider a scalar field $T(\underline{x})$ with maximum value at $\underline{x} = 0$. For example, $T(\underline{x})$ could be of the form

$$T(\underline{x}) = \frac{1}{p\,\|\underline{x}\|} \tag{2}$$

where p is a scalar constant. Next consider a simple point mass vehicle with the following equation of

motion

$$M\ddot{\underline{x}} = \underline{f} - k_{\dot{\underline{x}}}\,\dot{\underline{x}}\ , \tag{3}$$

with mass-matrix M, input vector $\underline{f}$ and linear drag coefficient $k_{\dot{\underline{x}}}$. Since $\underline{f}$ can only be a function of the measurable quantities such as $T(\underline{x})$ and $\nabla T_{\dot{\underline{x}}}$ we implement the following control input

$$\underline{f} = k\,T(\underline{x})^{-2}\,\nabla T_{\dot{\underline{x}}}\,\frac{\dot{\underline{x}}}{\|\dot{\underline{x}}\|}\,. \tag{4}$$

where k is a constant scalar. To study stability of the equilibrium $\underline{x} = 0$, $\dot{\underline{x}} = 0$, consider the Lyapunov function

$$V(\underline{x},\dot{\underline{x}}) = \frac{1}{2}\dot{\underline{x}}^T\,M\,\dot{\underline{x}} + kT^{-1}(\underline{x}). \tag{5}$$

The time derivative of the above equation can be written as

$$\dot{V}(\underline{x},\dot{\underline{x}}) = \dot{\underline{x}}^T\,M\,\ddot{\underline{x}} - k\,T(\underline{x})^{-2}\,\nabla T\cdot\dot{\underline{x}}\ . \tag{6}$$

Substituting (1) and (3) into the above equation allows us to rewrite

$$\dot{V}(\underline{x},\dot{\underline{x}}) = -\dot{\underline{x}}^T\,k_{\dot{\underline{x}}}\,\dot{\underline{x}} + \dot{\underline{x}}^T\,k\,T(\underline{x})^{-2}\,(\nabla T\cdot\frac{\dot{\underline{x}}}{\|\dot{\underline{x}}\|})\,\frac{\dot{\underline{x}}}{\|\dot{\underline{x}}\|} - k\,T(\underline{x})^{-2}\,\nabla T\cdot\dot{\underline{x}}\ . \tag{7}$$

This equation can be further simplified to

$$\dot{V}(\underline{x},\dot{\underline{x}}) = -\dot{\underline{x}}^T\,k_{\dot{\underline{x}}}\,\dot{\underline{x}} + k\,T(\underline{x})^{-2}\,\nabla T\cdot\dot{\underline{x}} - k\,T(\underline{x})^{-2}\,\nabla T\cdot\dot{\underline{x}} \tag{8}$$

and hence the system is stable since

$$\dot{V}(\underline{x},\dot{\underline{x}}) = -\dot{\underline{x}}^T\,k_{\dot{\underline{x}}}\,\dot{\underline{x}} \le 0 \tag{9}$$

for a positive definite $k_{\dot{\underline{x}}}$. However, while the velocity $\dot{\underline{x}}$ is guaranteed to converge to $\dot{\underline{x}} = 0$, we cannot conclude that the position converges to $\underline{x} = 0$. The vehicle will converge to some position that corresponds to a local maximum of T along the line defined by the vehicle's initial velocity. Note that the single vehicle will not turn under this control law.

Figure 3 in Section 2.5 shows the vehicle converging on the origin for the special case that the vehicle's initial direction passes through the origin. In general, as shown in Figure 4, it is seen that the vehicle only converges to the maximum value along its initial path. Note that these simulations are intended to demonstrate convergence. It can be seen that further damping is warranted to attenuate the oscillations.

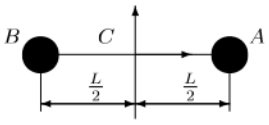

Figure 1: Masses connected by infinitely thin and stiff rod of length L.

2.4 Two-vehicle configuration

In this section we apply the control law developed in the previous section to the two-vehicle case. In order to simplify multi-vehicle configurations, we assume that the vehicles are able to hold their relative, preset inter-vehicle distance from one another. Control laws designed to maintain relative vehicle distance given measurements of relative position of neighbors are described in [7]. This simplifying assumption allows us to model the multi-vehicle problem as an ensemble of point masses connected by a weightless, stiff link. Here the two vehicle configuration is approximated by two linked point masses. Each point mass represents a vehicle. The equation of motion for vehicle A is

$$\frac{M}{2}\,\ddot{\underline{x}}_A \quad = \quad \underline{f}_A - k_{\dot{\underline{x}}}\,\dot{\underline{x}}_A\ . \tag{10}$$

where

$$\underline{x}_A = \begin{bmatrix} x_A \\ y_A \\ 0 \end{bmatrix} \tag{11}$$

is the position of vehicle A.

The position of vehicle A in local coordinates with respect to the origin of a local coordinate frame C (fixed on the linked-mass system) is denoted by $\underline{x}_A^C$. Let $\underline{x}_C$ denote the global position of the origin of frame C. Then, we can represent the vehicle's global position $\underline{x}_A$ in terms of the local position $\underline{x}_A^C$ using a rotation and translation

$$\underline{x}_A = R(\theta)\cdot\underline{x}_A^C + \underline{x}_C \tag{12}$$

where $R(\theta) \in SO(3)$ is a rotation matrix. Similarly, we write for any other (identical) vehicle B

$$\frac{M}{2}\ddot{\underline{x}}_B = \underline{f}_B - k_{\dot{\underline{x}}}\,\dot{\underline{x}}_B \tag{13}$$

and

$$\underline{x}_B = R(\theta)\cdot\underline{x}_B^C + \underline{x}_C. \tag{14}$$

In the case of a simple two-mass system we choose the local position vector of the point masses to be $\underline{x}_A^C =$

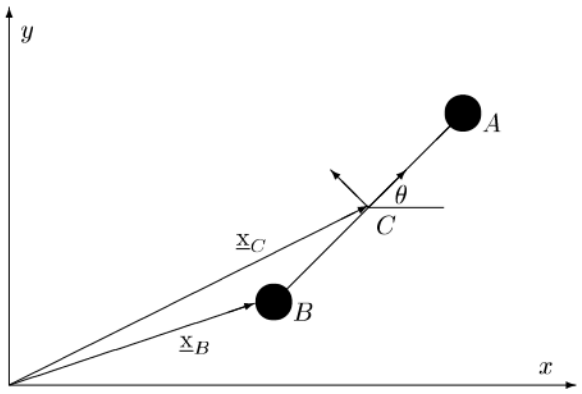

Figure 2: Coordinate systems for connected mass system.

$\begin{bmatrix} \frac{L}{2} \\ 0 \\ 0 \end{bmatrix}$ and $\underline{x}_B^C = \begin{bmatrix} -\frac{L}{2} \\ 0 \\ 0 \end{bmatrix}$ as shown in Figure 1. The coordinate systems for the connected mass system are shown in Figure 2.

The absolute velocities of masses A and B can be written as

$$\dot{\underline{x}}_A = R(\theta) \cdot (\underline{\omega} \times \underline{x}_A^C) + \dot{\underline{x}}_C \quad (15)$$

$$\dot{\underline{x}}_B = R(\theta) \cdot (\underline{\omega} \times \underline{x}_B^C) + \dot{\underline{x}}_C \quad (16)$$

with

$$\underline{\omega} = \begin{bmatrix} 0 \\ 0 \\ \dot{\theta} \end{bmatrix}.$$

The equations of motion for the two-mass system become

$$\begin{aligned} M\ddot{\underline{x}}_C &= \underline{f}_A - k_{\dot{\underline{x}}}\,\dot{\underline{x}}_A + \underline{f}_B \\ &- k_{\dot{\underline{x}}}\,\dot{\underline{x}}_B \\ I\dot{\underline{\omega}} &= (\underline{x}_A - \underline{x}_C) \times (\underline{f}_A - k_{\dot{\underline{x}}}\,\dot{\underline{x}}_A) \\ &+ (\underline{x}_B - \underline{x}_C) \times (\underline{f}_B - k_{\dot{\underline{x}}}\,\dot{\underline{x}}_B) \end{aligned}$$

where I is the system inertia. If we now implement the control law (4) from the single-vehicle case, such that

$$\begin{aligned} \underline{f}_A &= k\,T(\underline{x}_A)^{-2}\,\nabla T_{\dot{\underline{x}}_A}\,\frac{\dot{\underline{x}}_A}{\|\dot{\underline{x}}_A\|} \\ \underline{f}_B &= k\,T(\underline{x}_B)^{-2}\,\nabla T_{\dot{\underline{x}}_B}\,\frac{\dot{\underline{x}}_B}{\|\dot{\underline{x}}_B\|} \end{aligned} \quad (17)$$

then we obtain the following controlled system equations:

$$\begin{aligned} M\ddot{\underline{x}}_C &= k\,T(\underline{x}_A)^{-2}\,\nabla T_{\dot{\underline{x}}_A}\,\frac{\dot{\underline{x}}_A}{\|\dot{\underline{x}}_A\|} \\ &\quad -k_{\dot{\underline{x}}}\,\dot{\underline{x}}_A + k\,T(\underline{x}_B)^{-2}\,\nabla T_{\dot{\underline{x}}_B}\,\frac{\dot{\underline{x}}_B}{\|\dot{\underline{x}}_B\|} \\ &\quad -k_{\dot{\underline{x}}}\,\dot{\underline{x}}_B \\ I\dot{\underline{\omega}} &= (\underline{x}_A - \underline{x}_C) \times (k\,T(\underline{x}_A)^{-2}\,\nabla T_{\dot{\underline{x}}_A}\,\frac{\dot{\underline{x}}_A}{\|\dot{\underline{x}}_A\|} \\ &\quad -k_{\dot{\underline{x}}}\,\dot{\underline{x}}_A) \\ &\quad +(\underline{x}_B - \underline{x}_C) \times (k\,T(\underline{x}_B)^{-2}\,\nabla T_{\dot{\underline{x}}_B}\,\frac{\dot{\underline{x}}_B}{\|\dot{\underline{x}}_B\|} \\ &\quad -k_{\dot{\underline{x}}}\,\dot{\underline{x}}_B). \end{aligned} \quad (18)$$

2.5 Simulations

In this section we show simulation results for both the single as well as the dual-vehicle case. The simulations were performed using a scalar field $T(\underline{x})$ with

$$T(\underline{x}) = \frac{1}{p\,\|\underline{x}\|}. \quad (19)$$

Figure 3 shows a simulation of a single vehicle starting on the y-axis with an initial velocity in the direction of the origin. The figure on the left hand-side shows a view of the x-y plane with the vehicle's position (red-circle) at different instances in time. The right hand side shows the y-coordinate of the vehicle converging to the origin. This represents a special case, where the vehicle was already on an intersecting path with the origin. Figure 4 shows simulation results for a single vehicle starting off in a direction not intersecting with the origin. The left hand side shows the vehicle's position in the x-y plane. Since the vehicle starts off in a different direction than one that passes through the origin, it does not converge to the origin. The right figure shows a graph displaying the magnitude of the scalar field along the vehicle's path. The vehicle converges to the maximum of the magnitude along its path.

Next we implemented the control algorithm as described in Section 2.4. Figure 5 shows the results of the simulation. The red solid line indicates the position of the centroid of the two masses. Vehicles A and B are symbolized by a red and a green filled circle, connected by a blue line. The plot shows the position of the point masses in the x-y plane at different instances in time. The simulation shows that in the two-vehicle case the vehicles climb the gradient despite an initial direction that doesn't intersect the origin. This is not possible for a single vehicle unless it started off in the right direction.

3 Experimental test-bed

In this section we describe the development of an experimental test-bed to conduct multi-vehicle experiments in a laboratory environment. In particular,

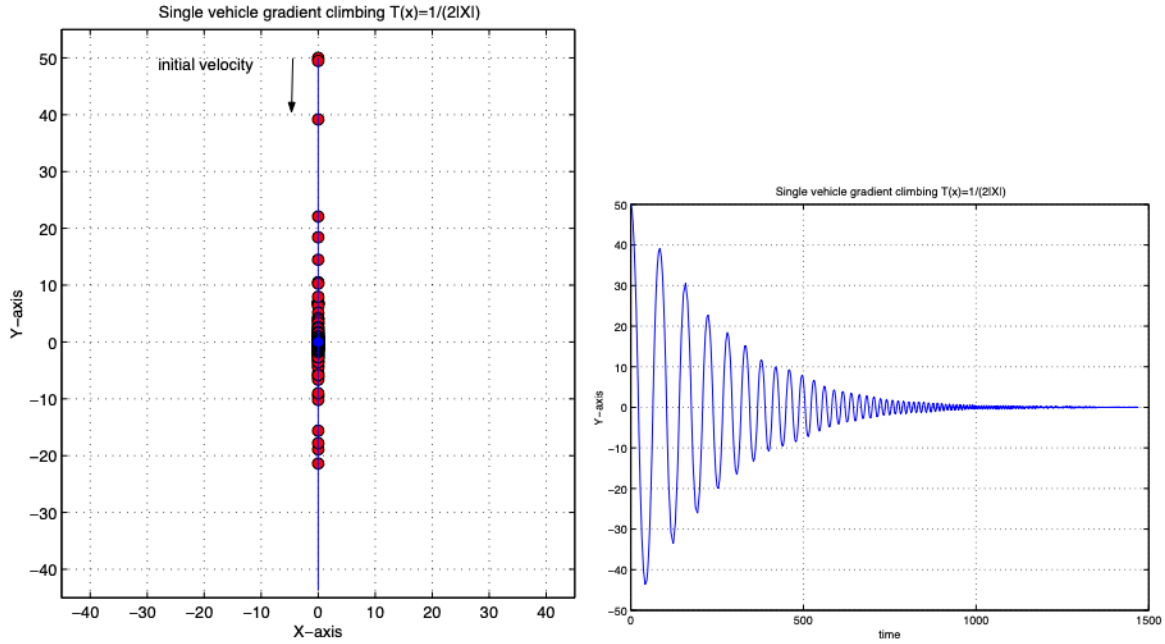

Figure 3: Simulation results for a single vehicle climbing the gradient with initial velocity vector intersecting with the origin.

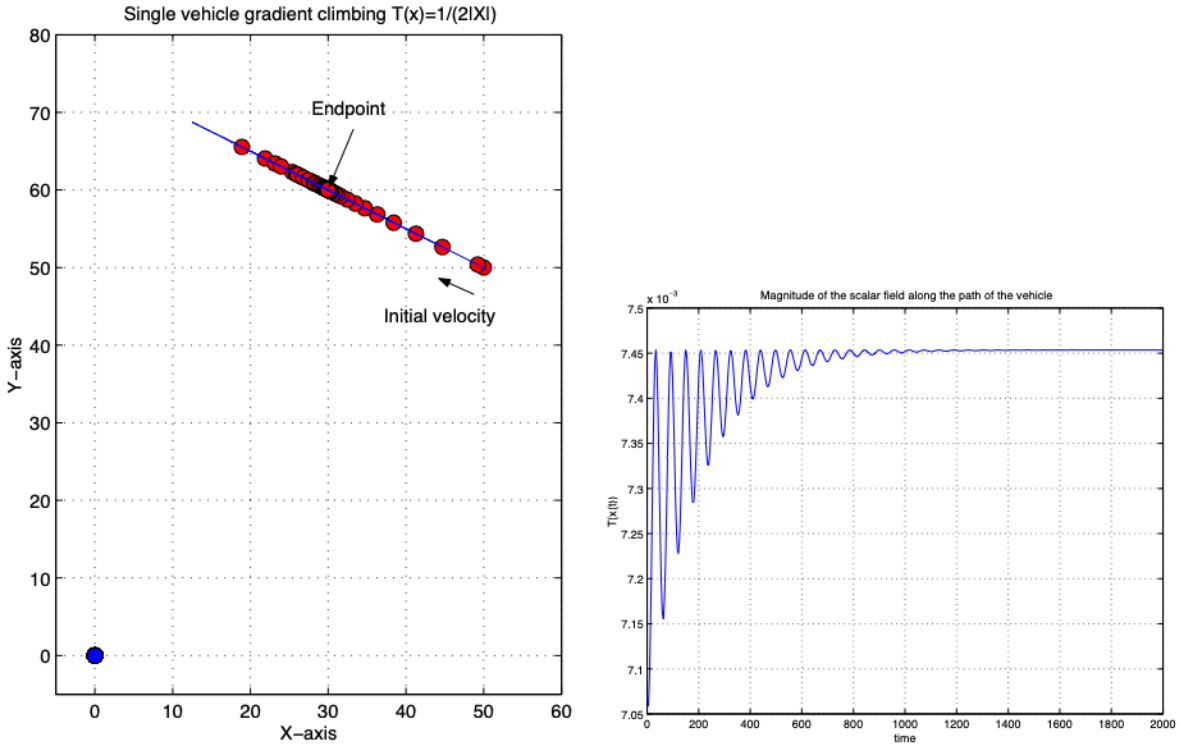

Figure 4: Simulation results for a single vehicle climbing the gradient with initial velocity vector not intersecting with the origin.

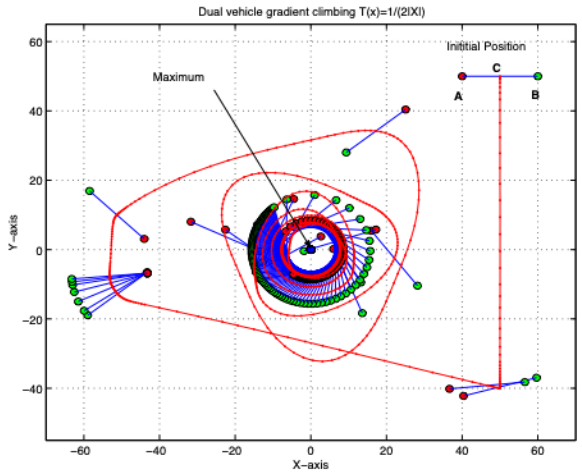

Figure 5: Simulation results using two vehicles climbing the gradient.

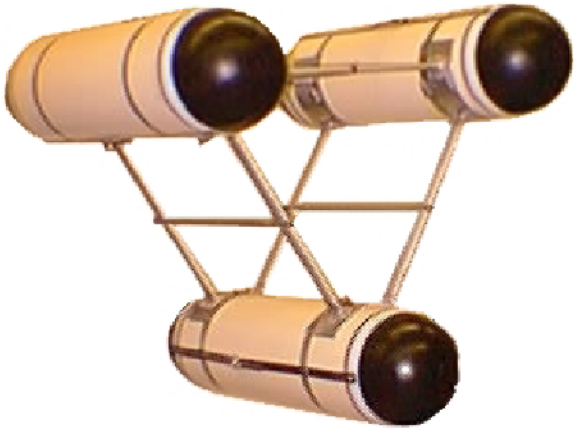

Figure 6: Picture of prototype vehicle.

we present details on the prototype "grouper" vehicle design.

3.1 System requirements

The multi-vehicle experimental system is being designed for an indoor laboratory so that we can operate in a filtered, high visibility, freshwater environment. Measurements that are critical for performing closed-loop decentralized vehicle network control experiments include

- global position and orientation of each vehicle
- relative position and orientation of each vehicle's nearest neighbors.

The relative position and orientation measurements are fundamental to group coordination strategies. The global position and orientation measurements will be useful for missions such as sampling, gradient climbing, etc.

The maximum design depth was set to be $10m$ and the vehicles are expected to be able to sustain a mean forward velocity of $0.25\frac{m}{s}$. In order to operate multiple vehicles in our free standing cylindrical tank (diameter 21ft, depth 8ft), the vehicles have to be compact and robust. In designing the vehicles special attention was given to the reliability of the components and expandability and evolution of the overall system in order to be able to accommodate new sensors and actuators without major redesign. In order to easily accommodate a variety of controllers to be tested, we have emphasized user friendliness of the higher level control interface. In the following we describe how we addressed or are planning to address these design challenges.

3.2 Mechanical layout

The design of the prototype "grouper" vehicle was chosen to provide good stability in pitch and roll. This choice simplifies the instrumentation and enables us to focus on the control of the remaining four degrees of freedom (4 DOF). The configuration is a variation of previous underwater vehicles such as *EAVE*[1] designed by the Autonomous Undersea Systems Institute (AUSI) and *ABE*[2] designed by Woods Hole Oceanographic Institution (WHOI). Figure 6 shows a picture of the prototype vehicle. The vehicle is $60cm$ long and its three pressure housings are arranged in a equilateral triangle with a side-length of $45cm$. The main bodies of the pressure housings consist of standard PVC piping with acrylic O-ring sealed end-caps. The connecting structure is made out of airfoil shaped extruded aluminum. The fairings of the pressure housings are hemispherical and made out of PVC.

3.3 System architecture

The main goal of the project to examine decentralized control of multi-vehicle configurations penetrates into the entire system design. On our prototype vehicle, we have implemented a distributed control system using a single RS-485 communication bus operating at 115.2kbaud with a standard communication protocol, *IEEE 997-1985*, also known as the *SAIL* standard [3]. This choice provides the flexibility of adding devices that implement the same standard with minimal or

[1] Experimental Autonomous VEhicles
[2] Autonomous Benthic Explorer

no changes in software and hardware. Due to the minimal requirements for the implementation of the protocol, all sensors and actuators are equipped with a low-power PIC16F873[3] 8-bit flash microcontroller for direct addressing, data communication and basic signal processing. The bus master is currently the surface station that sends and requests information to and from the appropriate nodes of the network. In a next step this bus master will be implemented using a single board computer (SBC) in the vehicle itself. Figure 7 illustrates this next step for implementing the vehicle network using a vehicle SBC and low bandwidth RF link. The RF-modem operating at 49MHz with a baudrate of up to 9600baud is planned to replace the communication tether.

Using the communication channel the control system can be implemented in different ways. One possible scenario is a strictly hierarchical structure where the surface computer issues direct commands to each individual vehicle and the SBC vehicle computer would just relay the communication to the sensors and actuators. This approach is severely limited by the available communication bandwidth and seems only feasible using a fixed tether, which excludes full 3D-multi-vehicle operations.

By moving more control authority into the vehicle, e.g., by just sending new setpoint information for the individual vehicle through the communication channel, we can accommodate more vehicles than in the previous case. In this scenario the surface computer would act as a supervisory controller for each individual controller while the on-board SBC would take the role of closing the loop by directly communicating with the sensors and actuators.

A third possible scenario could be one in which the vehicle only obtains information about other, e.g., neighboring vehicles, such as location and orientation with the appropriate formation and task specific control laws implemented on the vehicle level. This latter scenario would make the surface computer a mere observer of the group and would shift all control authority to the vehicle level. This approach would make it possible to use the available communication channel for inter-vehicle communication in order to enhance group coordination.

3.4 Sensors and actuators

In this section we discuss the sensors and actuators that are already on or are planned to be used on the vehicle or in the tank.

The vehicle is actuated using geared DC-brushed

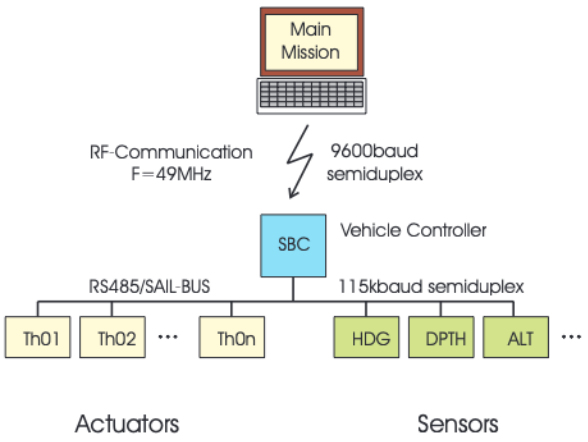

Figure 7: Computer network and communication.

Figure 8: Photo of a thruster motor.

motors[4] with 9in twin bladed propellers as shown in Figure 8. Each individual thruster can provide up to $12N$ of thrust under bollard-pull conditions. The motor-controller uses a full-bridge PWM motor driver chip[5] interfaced to the PIC processor. The motors are equipped with magnetic encoders that provide position feedback into a PIC microcontroller with a resolution of $896\frac{\text{counts}}{\text{rev}}$. The thrusters can be operated in velocity as well as torque mode.

For depth information the vehicle is equipped with a 5psi pressure depth sensor that interfaces to a 10bit AD converter on a PIC. A magnetic compass[6] pro-

[3]Microchip Technology Inc., Chandler, AZ, USA

[4]Series 2342, MicroMo Electronics, Inc.

[5]A3958SB Allegro MicroSystems,Inc.

[6]Vector 2X, PNI Corp., Santa Rosa, CA

vides magnetic heading information. However, while the vehicle is deployed in the steel tank the usefulness of the sensor as a heading reference is limited. In order to provide a more reliable heading reference we are installing a fiber optic gyro[7].

In parallel with the gyro and compass implementation, we have developed a prototype for an optical heading module. The optical heading module uses a 2D-position sensitive device (PSD) on the vehicle and an array of sequenced blinking LEDs on the bottom of the tank, not unlike the running lights on a runway. The system works well in air at a distance of up to $2m$ and preliminary tests in water are promising. The prototype system provided sensor readings up to $1.5m$. The same system is planned to be used for near neighbor position sensing [6].

In order to obtain global position information we are currently considering two different systems: a 40kHz acoustic long baseline system[8] and a variation of the above described optical heading module. The acoustic system was made available for testing by the manufacturer. We used the standard system with a transducer and a single transponder to obtain range information in our free standing steel tank. The update-rate was at 1Hz. The free-standing tank environment represents the worst-case scenario for the acoustic system. The walls represent a good reflector for the acoustic waves and the operating frequency of 40kHz does not significantly decay over the length-scale of the tank. The transponder was mounted $0.5m$ from the edge of the tank and the receiver close to the center of the tank. The ranges were recorded using the Desert Star tracking software. The system performed within the manufacturer's specifications of a $0.15m$ standard deviation.

As an alternative to the acoustic system we are exploring the possibility of using the above described optical system for absolute position information. The fast response time of the PSD has the potential for a high position update rate and a higher accuracy but has a limited range that makes it unusable in open water application.

3.5 Preliminary experimental data

In order to evaluate the existing system we did some preliminary testing of the control system. We implemented a depth servo controlling the vertical thruster. The servo read the pressure sensor from the surface computer (PC 166MHz) via the communication tether using the standard Matlab[9] serial communication interface at 115.2kbaud with no real-time extension or acceleration option. The software control loop consists of four parts:

1. read depth sensor (one serial write and read process)
2. read motor rpm (one serial write and read process)
3. calculate motor command (PID controller)
4. send motor command (one serial write process).

Figure 10 shows the results of one of the experiments with a desired depth of $1.73m$. The vehicle is slightly heavy. It started off from the bottom and reached the setpoint after $60s$ with disturbances due to the tether. One of the objectives of this test was to determine the update rate this basic setup could provide as a future benchmark. Figure 11 shows the time between two update cycles of the servo-loop at an average of $0.28s$. By implementing the control loop on a 1GHz Pentium III we have observed an increase in speed by a factor of 5. With the current setup we are able to perform closed-loop depth control at a sufficiently high update rate but for additional tasks such as auto-heading or position control this setup is inadequate. As a solution to this problem we consider the option of implementing the basic controllers, such as the depth and heading controllers either on the vehicle's SBC or directly on the actuator and sensor level of the vehicle.

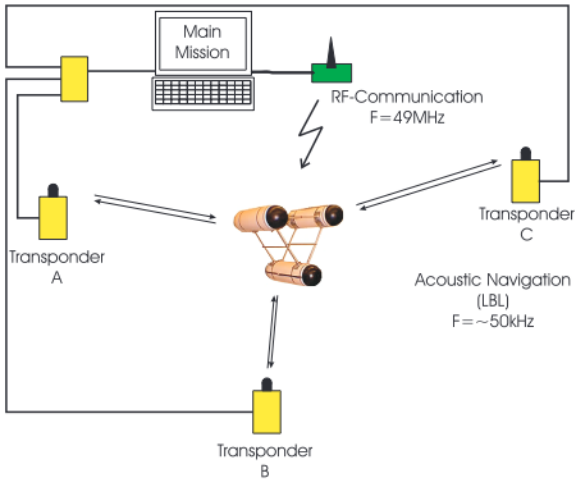

Figure 9: Acoustic navigation scheme.

[7] E-core 1000, KVH Industries, Inc., Middletown, RI
[8] Desert Star Systems LLC., Marina, CA
[9] The MathWorks, Inc., Natick, MA

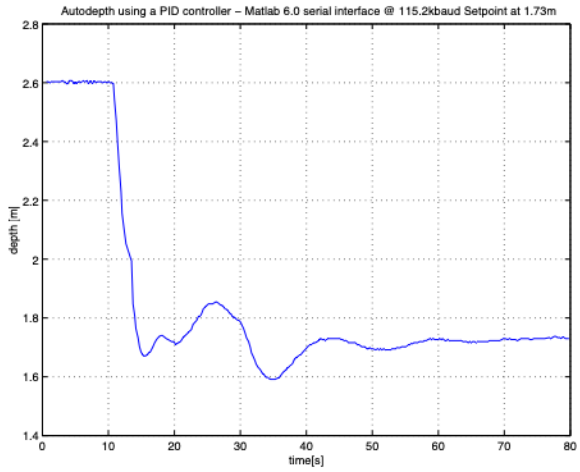

Figure 10: Vehicle depth in meters versus time using a closed loop PID controller implemented using the standard Matlab 6.0 serial interface.

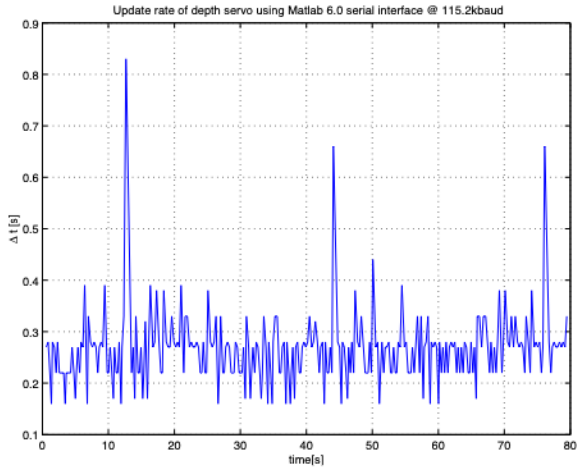

Figure 11: Update rate in seconds of the PID depth control loop.

4 Conclusions and future work

In the first part of the paper we showed a potential benefit of a multi-vehicle configuration in the context of gradient climbing. We designed a stable continuous controller for a single vehicle that allowed the vehicle to find a maximum along its initial direction of motion. The same controller was then tested in a two -vehicle simulation, under the assumption of a strong interaction between the vehicles. We showed in simulation that the two vehicles climb the gradient deviating from their initial direction of motion towards the maximum. In a next step we will look into stability properties of the two-vehicle controller. The question of scalability also arises, and we plan to investigate controller performance with a larger number of vehicles. We also plan to explore a larger variety of scalar fields and to address how best to manage undesirable local maxima. Before the controller can be implemented and tested on the actual system, some assumptions have to be reviewed, i.e. the interaction between the vehicles has to be represented by a more realistic model. In particular, control terms need to be included to guarantee a constant range between neighboring vehicles. This problem has been addressed in [7] and we plan to incorporate the approach into a multi-vehicle controller. The developments on orientation alignment of multiple underwater vehicles in [13] may also prove useful.

In the second part of this paper we gave an overview of the experimental setup with the existing infrastructure and gave a brief example of a PID-depth controller. We are continuing the implementation of a variety of additional off-the-shelf sensors, such as the fiber optic gyro, a long baseline acoustic navigation system and a acoustic doppler velocity-meter (ADV). Besides these off-the-shelf components, we are continuing to work on the optical heading module with its possible variations. In parallel with the upgrading of the prototype, we are planning to build 2-3 more vehicles this year. Other plans include incorporating our laboratory-scale underwater glider into grouping control designs and experiments [8].

5 Acknowledgements

We would like to thank Edward Fiorelli for his input and help during all stages of the project. Further we would like to thank Kaijen Hsiao and Probal Mitra for their valuable work on the optics and electronics of the PSDs.

References

[1] J. Adler. Chemotaxis in bacteria. *Science*, 153(3737):708–716, August 1966.

[2] H. C. Berg. *Random Walks in Biology*. Princeton University Press, Princeton, NJ, 1983.

[3] A. Bradley. The sail standard. Technical report, WHOI, June 1998.

[4] E. Burian, D. Yoerger, A. Bradley, and H. Singh. Gradient search with autonomous underwater vehicle using scalar measurements. *Proceedings of the IEEE OES AUV conference, Monterey, California*, June 1996.

[5] D. A. Hoskins. A least action approach to collective behavior. *Microrobotics and Micromechanical Systems*, Proc. SPIE 2593:108–120, 1995. Lynne E. Parker, Editor.

[6] K. Hsiao. Inter-vehicle position/orientation determination for multiple autonomous underwater vehicles. Independent Work Report, Princeton University, May 2001.

[7] N. Leonard and E. Fiorelli. Virtual leaders, artificial potentials and coordinated control of groups. In *Proc. IEEE Conference on Decision and Control*, 2001. To appear.

[8] N. Leonard and J. Graver. Model-based feedback control of autonomous underwater gliders. *IEEE Journal of Oceanic Engineering, Special Issue on Autonomous Ocean Sampling Networks*, 2001. In press.

[9] A. MacDonald. Autonomous survey teams. *Underwater Intervention*, January 2001.

[10] J. G. Northcutt, A. A. Kleiner, and T. S. Chance. A high-resolution survey AUV. *Offshore Technology Conference*, May 2000.

[11] A. Okubo. Dynamical aspects of animal grouping: Swarms, schools, flocks and herds. *Advances in Biophysics*, pages 1–94, 1985.

[12] J. K. Parrish and W. H. Hammer, editors. *Animal Groups in Three Dimensions*, page 378. Cambridge University Press, 1997.

[13] T. Smith, H. Hanssmann, and N. Leonard. Orientation control of multiple underwater vehicles with symmetry-breaking potentials. In *Proc. IEEE Conference on Decision and Control*, 2001. To appear.

[14] M. A. Tivey, H. P. Johnson, A. Bradley, and D. R. Yoerger. Thickness of a submarine lava flow determined from near-bottom magnetic field mapping by an autonomous underwater vehicle. *Geophysical Research Letters*, 25(6):805–808, March 1998.

[15] D. R. Yoerger, A. M. Bradley, M.-H. Cormier, W. B. F. Ryan, and B. B. Walden. Fine-scale seafloor survey in rugged deep-ocean terrain with an autonomous robot. *IEEE ICRA*, April 2000.